



## Review

# Single molecule force spectroscopy in biology using the atomic force microscope

Jordanka Zlatanova<sup>a,\*</sup>, Stuart M. Lindsay<sup>b</sup>, Sanford H. Leuba<sup>c</sup><sup>a</sup> *Biochip Technology Center, Argonne National Laboratory, 9700 South Cass Avenue, Bldg. 202-A253, Argonne, IL 60439, USA*<sup>b</sup> *Department of Physics and Astronomy, Arizona State University, Tempe, AZ 85287, USA*<sup>c</sup> *Physical Molecular Biology, Laboratory of Receptor Biology and Gene Expression, National Cancer Institute, NIH, Building 41, Room B507, Bethesda, MD 20892, USA*

---

**Abstract**

The importance of forces in biology has been recognized for quite a while but only in the past decade have we acquired instrumentation and methodology to directly measure interactive forces at the level of single biological macromolecules and/or their complexes. This review focuses on force measurements performed with the atomic force microscope. A general introduction to the principle of action is followed by review of the types of interactions being studied, describing the main results and discussing the biological implications. Published by Elsevier Science Ltd.

*Keywords:* Atomic force microscopy; DNA stretching; Intermolecular interactions; Intramolecular interactions; Protein unfolding; Single molecule force spectroscopy

---

**Contents**

1. Introduction . . . . .	38
2. The AFM for force measurements . . . . .	38
2.1. Principle of action . . . . .	38
2.2. General requirements for sample preparation and deposition . . . . .	43
3. Intermolecular interactions . . . . .	44
3.1. Receptor/ligand interactions . . . . .	45

---

\*Corresponding author. Present address: Chemical Engineering, Chemistry and Materials Science Department, Polytechnic University, Brooklyn, NY 11201, USA. Tel.: +1-718-260-3176; fax: +1-718-260-3125.

*E-mail address:* jzlatano@duke.poly.edu (J. Zlatanova).

3.2. Protein/protein interactions . . . . .	49
3.3. Interactions between complementary strands of DNA . . . . .	49
3.4. Stretching chromatin . . . . .	50
4. Intramolecular structural transitions in polysaccharides, DNA, and multi-domain proteins . . .	50
5. Measuring the viscoelastic properties of biological structures and macromolecules . . . . .	54
6. Measuring interactions between cells . . . . .	55
7. Force maps . . . . .	56
8. Concluding remarks . . . . .	56
Acknowledgements . . . . .	56
References . . . . .	56

## 1. Introduction

Understanding the forces that govern specific molecular interactions is a challenging task in molecular and structural biology. Such specific interactions result from multiple weak, non-covalent bonds formed between defined portions of the interacting molecular partners. Various techniques have been recently employed to directly probe such weak interactions, including surface force apparatus (Israelachvili, 1992), pipette suction (Evans et al., 1991), magnetic beads (Smith et al., 1992), flow chamber apparatus (Pierres et al., 1996), and optical traps and tweezers (Ashkin et al., 1987; Ashkin, 1997). The techniques using optical traps have been particularly popular in view of their high force sensitivity. The disadvantages of the optical trap-based apparatuses are in the limited range of samples amenable to analysis (biopolymers must be generally longer than  $\sim 2\ \mu\text{m}$ ), and general unsuitability for applying forces greater than  $\sim 150$  piconewtons (pN).

The advent of the probe microscopes, and in particular the atomic force microscope (AFM) (Binnig et al., 1986) has opened new horizons in force measurements. This review will focus on the use of AFM to study inter- and intramolecular interaction forces in biological macromolecules. It will also briefly illustrate the use of the techniques to evaluate mechanical properties of biological samples, like elasticity and viscosity.

## 2. The AFM for force measurements

### 2.1. Principle of action

The AFM (Fig. 1A) uses a sharp tip mounted at the end of a flexible cantilever to probe a number of properties of the sample, including its topological features and its mechanical characteristics. Precise lateral and vertical displacement of the sample with respect to the probe is achieved by a computer-controlled piezoceramics stage holding the sample, or conversely, the cantilever holder. Forces acting between the surface and the probe cause deflection of the

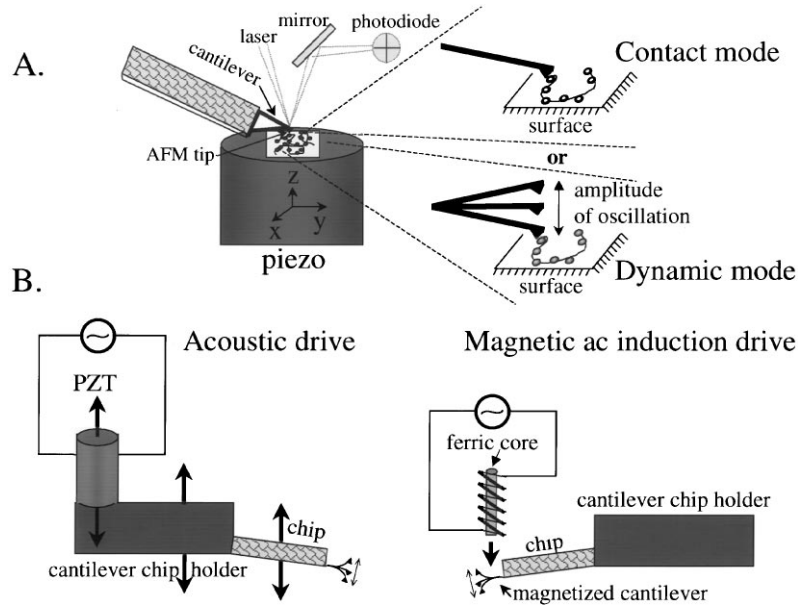


Fig. 1. Schematic of the principle of action of the atomic force microscope (A). The enlargements on the right-hand side illustrate the principle of the static mode (top) and the dynamic mode (bottom) of action. (B) Illustration of the acoustic and the magnetic-oscillation-induction dynamic modes of action.

cantilever that is registered by a laser beam reflected off the back of the cantilever. The cantilever deflections are used to create a topographic image of the sample when the probe is raster-scanned in the  $x$ - $y$  direction, or to produce the so-called force curves, when the probe is moved in the  $z$ -direction, i.e., first moved downwards until it contacts the surface, and then upwards, till no interaction between probe and surface is felt. The resultant plot of cantilever deflection versus the separation between the probe and the sample is the force curve. The AFM combines high force sensitivity (down to a few pN) with high lateral resolution (often better than a nanometer, which is in the realm of molecular dimensions).

The high resolution of forces (for a detailed discussion see Sarid, 1991) results from the small spring constants of the cantilever (usually in the range of 0.5–0.01 N/m) to which the tip interacting with the sample is attached. The force sensitivity is limited by the stiffness of the cantilever and the laser power. The main noise contributions come from thermal excitation of the cantilever motion, the intensity distribution in the laser beam, and the bandwidth (the range of frequencies over which the signal is collected) (i.e., a slow pulling with limited bandwidth will give better signal-to-noise ratio, the noise being proportional to the square root of the bandwidth).

The high spatial resolution is achieved through the use of very sharp probes.

There are two different modes of operation of the AFM in its force recording regime (Fig. 1A). In the static (contact) mode, the tip approaches the surface, is pushed into the surface, and is then retracted by the piezo stage. In the dynamic mode, the cantilever is oscillated while it is moved to and from the surface. The measured parameter is the reduction in the amplitude of oscillation that is caused by the interaction of the tip and the surface.

There are two general methods to oscillate the cantilever, acoustical or magnetic (Fig. 1B). In acoustic, or ‘tapping’ mode (Zhong et al. (1993); for extension of this method to fluids see Hansma et al. (1994) and Putman et al. (1994)), the cantilever is oscillated above the surface near its resonance frequency. The second method uses a magnetic alternating current (ac) field to oscillate the cantilever that is coated with a thin magnetically susceptible film (for a recent detailed comparison of the two methods, see Lindsay, 2000).

A typical force versus displacement curve generated by an AFM is shown in Fig. 2. At the beginning, the probe is far away from the surface, so there is no interaction between the two (Fig. 2). As the probe–sample separation is reduced beyond a certain point, forces between atoms on the two surfaces begin to act, causing the flexible cantilever to bend toward the sample in the case of attractive forces (van der Waals and electrostatic), or away from the sample in the case of repulsive forces (electrostatic). At each distance, the cantilever bends until its elastic (restoring) force equals the probe–sample interaction force and the system is in equilibrium. The attractive forces can cause the probe to snap to the surface earlier (from a greater distance) than the expected time of contact in the absence of such forces. (Contact may be defined as the point when repulsion is first detectable.) The jump-to-contact observed in approach curves limits the range of data that may be obtained on the approach cycle and also the gentleness of the tip approach.

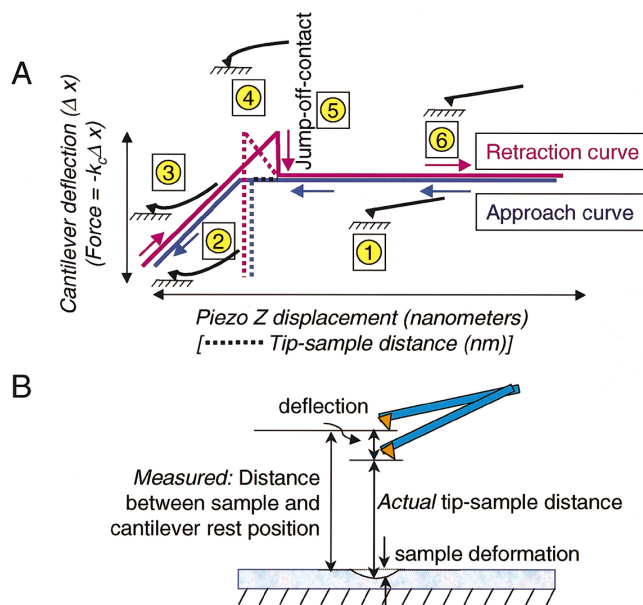


Fig. 2. Schematics of types of force curves and tip–sample interactions. (A) Typical contact force versus  $Z$  displacement curve generated by an AFM, and (B) schematic of the tip/sample interaction. In (A) the deflection of the cantilever is shown as a function of the piezo  $Z$  displacement. The numbers correspond to different states of the cantilever during the approach and retraction portions of the cycle: (1) AFM tip is not in contact with surface; (2) tip is being pushed into the surface, bending the cantilever; (3) tip is being withdrawn from the surface; (4) tips adheres to sample surface; (5) tip ‘jumps-off-contact’ from surface; (6) tip is not in contact with surface. The schematic in (B) of the tip–sample interaction is used to illustrate why there is a difference between the force versus piezo  $Z$  displacement curve [solid lines in (A)], and force versus tip–sample distance curve [dotted lines in (A)].

When the jump-to-contact is caused by electrostatic attraction, it can be minimized by operating in electrolytes that screen these interactions (Müller and Engel, 1997). Once in contact with the surface, the probe will experience an ever-increasing repulsive force (and the cantilever will bend away from the surface) as the electron orbitals of the atoms in the probe and the sample will begin to overlap. In this region of the force curve, referred to as the contact region, there may be elastic and/or plastic (reversible and/or irreversible) deformations of either or both the probe and the sample. These deformations may give additional information about the mechanic properties of the experimental sample, as will be discussed below.

As described by numerous authors (for recent reviews and references therein see Noy et al., 1997b; Heinz and Hoh, 1999a; Cappella and Dietler, 1999), there is a distinction between the force versus piezo  $Z$  displacement curve recorded by the AFM and the force versus tip–sample distance curve. We illustrate this distinction in Fig. 2 which shows that the actual tip–sample distance is the difference between the piezo  $Z$  displacement and the deflection of the cantilever (with soft samples, sample deformation needs to be taken into account too, see Section 5). At zero force, the points in both types of curves coincide; the maximum difference between the two plots is at the maximum force. When pulling long molecules like titin or chromatin fibers, the sample deformation at the surface and the cantilever deflection distance are negligible compared to the distance the tip travels up and down: thus, the difference between piezo  $Z$  displacement and tip/sample distance can be safely ignored.

Next, after a preset value of load is reached, the direction of motion is reversed and the probe moves away from the surface. During retraction of the probe, there may be manifestation of other forces: adhesion forces, created during contact and, in some specific cases, hydrophobic and solvation forces (Fig. 3). Of special interest to us is the adhesion force that is estimated from the deflection of the cantilever right before the jump-off-contact point. Jump-off-contact occurs when the effective elastic constant of the cantilever overcomes the adhesive interactions between probe and sample. Although the precise thermodynamic entity that is correlated to the adhesion force measured at jump-off-contact is still under discussion (see Moy et al., 1994a; Chilkoti et al., 1995), it is clear that this force can be used to compare interaction strength of different atomic arrangements within molecules or between molecules. The cantilever deflections occurring as a result of interatom interactions are converted into force using Hooke's law:

$$F = -k_c d,$$

where  $F$  is the force acting on the cantilever,  $k_c$  is the spring constant of the cantilever, and  $d$  is its deflection. There is considerable spread in the values of cantilever force constants and independent calibration is essential. Various authors have described different methods for calculating the spring constant. In one of these approaches, the spring constant is calculated from the cantilever geometry (Sader and White, 1993; Sader, 1995; Chen et al., 1994, 1995). This approach, however, assumes that the material properties of the thin films used in the manufacture of cantilevers are stable, reproducible, and known. Another set of approaches relies on measuring static deflection in response to a known force (Senden and Ducker, 1994; Torii et al., 1996; Gibson et al., 1996). Yet a third approach measures changes in dynamical properties of vibrating cantilevers (Hutter and Bechhoefer, 1993; Cleveland et al., 1993; Sader et al., 1995). We have found the static methods to be the most straightforward (Li et al., 1993).

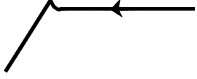
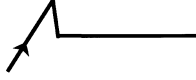
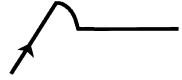
Force	Description	Shape of Curve
<b>From approach curve</b>		
Attractive van der Waals force	Creates jump-to-contact peak; depends on force between tip and sample and the system geometry; Meniscus forces must be eliminated by working in a low humidity environment or in liquid	
Repulsive double-layer electrostatic force	Due to charging both sample and tip surfaces with like charges (adsorption of ions from solution and dissociation of functional groups on surfaces)	
Repulsive hydration force	Comes from repellant interactions between hydrated ions bound to tip and sample surfaces; apparent at high salt concentration	
Solvation force	When tip and sample are within a few molecular diameters from each other, oscillation between attraction and repulsion may be observed; caused by ordering of non-polar liquid molecules between the two liquid-solid interfaces; force follows density of solvent	
<b>From retraction curve</b>		
Adhesion	Due to van der Waals forces and indentation of sample by tip (which increases contact area); Meniscus force must be eliminated	
Hydrophobic force	Appear on imaging hydrophobic samples in water; Results in a gradual pull-off instead of a jump-off-contact	

Fig. 3. Types of interaction forces felt by the cantilever during the approach and retraction portion of the force curve.

AFM force curves are rich in information (for reviews see Burnham et al., 1993; Cappella et al., 1997; Burnham and Kulik, 1998; Vinckier and Semenza, 1998; Heinz and Hoh, 1999a; Cappella and Dietler, 1999). They have allowed, among other things, measurements of the strength of individual hydrogen bonds (Hoh et al., 1992), and of different kinds of covalent bonds (Grandbois et al., 1999). Fig. 3 summarizes the types of forces sensed by the cantilever, and illustrates the effect of each type of interaction on the appearance of the force curve. In practice, force curves are rather complex since different forces may affect the behavior of the cantilever at any given value of probe/sample separation. This complexity requires specific care in the interpretation, the correctness of which depends on the results of sets of control experiments.

Although the dynamic mode presents several important advantages over the contact mode (Lindsay, 2000), the interpretation of contact force curves is rather straightforward (see below), whereas curves recorded in the dynamic mode are more difficult to interpret in terms of forces. It has been shown that the contact force curve is reproduced by integration of the oscillation amplitude curves when the forces are conservative, i.e., the process is reversible (Liu et al., 1999). In the event that the amplitude damping is purely a consequence of an elastic interaction (and dissipative processes do not contribute to it), the stiffness of the molecule is given by

$$S(z) = -k \left( \frac{A_0}{A(z)} - 1 \right), \quad (1)$$

where  $A_0$  is the undamped amplitude (typically  $\sim 5$  nm),  $A(z)$  is the amplitude at a distance  $z$ , and  $k$ , the spring constant of the cantilever. The force can be obtained from Eq. (1) by integration:

$$F(z) = -k \int \left( \frac{A_0}{A(z)} - 1 \right) dz + C. \quad (2)$$

Comparison of contact and magnetic ac curves may be extremely useful in the interpretation of the data, because, in the event that they reflect reversible, purely elastic processes, the two are simply related (Liu et al., 1999). Thus, the pair of curves recorded simultaneously serves to distinguish elastic from dissipative processes.

For biological applications tips are often modified to carry specific chemical groups or molecules, which allows assessing the weak van der Waals, electrostatic and hydration forces acting between the molecules on the tip and those on the surface. It is well established that a thin wetting film of liquid (water) covers both the probe and the sample when the AFM is operated in air (Grigg et al., 1992; Burnham et al., 1993; Burnham and Kulik, 1998). This thin film of water creates capillary forces that may have a dramatic effect on the force curves. The overall magnitude of the capillary force can be large enough to obscure the weak van der Waals forces. In view of this, experiments aimed at quantitation of interaction forces should be performed in liquids, in vacuum, or under dry nitrogen. Aqueous solution operation is desirable with biological molecules because it preserves their native structure.

The major parameter affecting bond rupture is the applied loading rate (the change of force with time —  $dF/dt$ ). Loading rate is also given as the product  $k_c v$  of the tip velocity,  $v$ , and the spring constant,  $k_c$ , of the cantilever (Evans and Ritchie, 1997). The probability of thermal rupturing of the bond increases as  $\exp(-[E_B - Fx_B]/k_B T)$ , where  $E_B$  is the potential energy barrier of bond disruption,  $F$  is the applied force in the bond direction,  $x_B$  is the stretched distance in this direction,  $k_B$  is the Boltzman constant, and  $T$  is the temperature. This description of loading rate applies if the loading force is generated by the cantilever alone. However, when the force is transmitted by a compliant polymer, the loading rate at some site (the bond to be ruptured) within that polymer also depends on the compliance and the extension of the polymer. Evans and Ritchie (1999) have illustrated this point on the example of the unfolding of a titin domain as a function of the pulling speed (Fig. 4), based on the original data from Rief et al. (1997a) and Kellermayer et al. (1997). The upper set of points (falling on the line in this log–log plot, Fig. 4) is for titin molecules of 500 nm in length. The lower cluster of data points is for longer molecules (several microns). The longer molecules generate a force that increases more slowly with time for the same overall pulling speed. When the internal loading rate is taken into account, the data fall on a universal line. Thus, comparison of bond-rupture or unfolding force data from various experiments requires control of both the external loading rate and the sample size (Evans and Ritchie, 1999).

## 2.2. General requirements for sample preparation and deposition

Studying biological macromolecules with the AFM puts several requirements to the way the sample is prepared and attached to the surface. Extreme care should be taken in using solutions of highest possible purity, since contamination may affect both imaging and force measurements. In addition, special attention should be paid to strongly attaching the molecules to the surface. Good

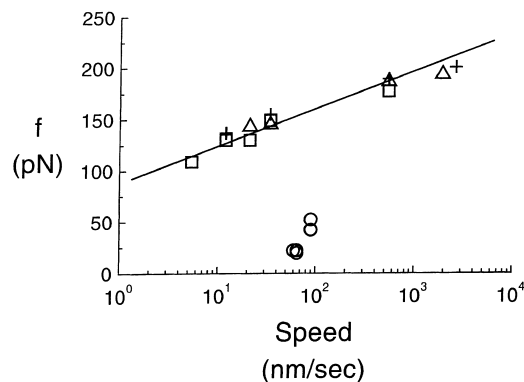


Fig. 4. Relationship of measured force of unfolding a titin domain as a function of pulling speed (Fig. 2 from Evans and Ritchie (1999), with permission of Biophysical Journal).

attachment is a must in this technique since the scanning probe may shift a weakly bound molecule around, thus precluding stable imaging or force registration. While the attachment should be firm enough to avoid undesired motions, it should still allow certain freedom of the molecule to change its conformation during biological activity or interaction with its molecular partners. Too firm an attachment along considerable portion of the molecular surface may lead to undesirable denaturing effects and should be avoided. The above requirements have resulted in considerable effort to properly attach molecules to the surface, both via non-specific adsorption and by covalent bonding. Recent useful descriptions of available techniques can be found in Tendler et al. (1996), Müller et al. (1997), Vinckier and Semenza (1998), Wagner (1998), Siedlecki and Marchant (1998), and Engel et al. (1999).

### 3. Intermolecular interactions

As mentioned above, it is possible to use the capability of AFM to sense interaction forces between atoms at the end of the probe and in the specimen to study the weak, non-covalent, usually short-range forces involved in molecular recognition reactions. In order to be able to do so, the partners in the molecular recognition reaction have to be immobilized onto the surface and the probe. Probes containing certain chemical functionalities can be used for mapping the spatial arrangement of chemical groups on a surface, in an approach termed *chemical force microscopy* (Frisbie et al. (1994); for a review see Noy et al. (1997b)). In this pioneering work from C. Lieber's laboratory it was demonstrated that probes functionalized with  $-\text{CH}_3$  or  $-\text{COOH}$  groups can specifically interact with similar groups on the surface, with the spatial pattern of interaction reproducing the spatial distribution of functional groups on the surface (Frisbie et al., 1994). A significant technological advance in chemical force microscopy was achieved by introducing covalently functionalized nanotubes as AFM probes (Wong et al., 1998). Nanotubes offer several important advantages over conventional AFM tips: they have high aspect ratio allowing probing of deep crevices, small effective radius increasing the lateral resolution of topographical and force

imaging, and are very flexible, avoiding the common problem of tip breakage. Functionalized nanotubes allowed chemically sensitive imaging of patterned samples, and more importantly in the context of this review, measuring interaction forces between biotin/streptavidin (Wong et al., 1998; Table 1).

Measuring intermolecular interactions between partners in molecular recognition reactions utilizes an analogous approach. It immobilizes each of the partners on either the probe or the surface, and then takes the probe through approach/retraction cycles. The magnitude of the cantilever deflection at the jump-off-contact peak is taken to reflect the rupture force needed to break the molecular interactions holding the two partners in close contact; breaking of the interaction bonds restores the cantilever to its neutral non-contact, non-deflected position.

There are several groups of intermolecular interaction forces experimentally measured with the AFM (Tables 1 and 2). Typical force curves recorded for each type of molecular pair are presented in Fig. 5, to facilitate perception of the characteristic features in each case and to allow comparisons. It must be noted that the specific intermolecular interactions are registered against the background probe/surface interactions, which may be as high as, or even higher, than the biological interaction of interest (Stuart and Hlady (1995); for further possible artifacts, see Stuart and Hlady (1999)). This requires careful choice of specificity controls. These generally include the use of non-functionalized probes or surfaces, blocking the interaction between the immobilized molecular partners with free ligands in the medium, or changing the pH or the salt concentration in the medium (for detailed information on specificity controls used in specific applications, see Tables 1 and 2).

### 3.1. *Receptor/ligand interactions*

A lot of experimental effort has gone into studying receptor/ligand interactions, on the example of the small ligand biotin interacting with the closely related proteins streptavidin or avidin. The biotin/streptavidin ligand/receptor pair has been used as a model system because of its unusually high affinity and the availability of structural and thermodynamic data. The interpretation of the force data has been greatly facilitated by the use of site-directed mutants of the receptor proteins, as well as of structural derivatives of biotin itself. As seen from Table 1, measurements from different laboratories, performed under a wide variety of experimental setups and conditions, agree pretty well, reinforcing the credibility of the AFM approach for force measurements.

The biotin/streptavidin system has been also utilized to study the dependence of the measured interaction forces on the loading rate. Evans and Ritchie (1997) (see also above) have argued, on the basis of theoretical considerations concerning bond rupture under application of force, that bond strength progresses through three dynamic regimes of loading rate: a slow-loading, a fast-loading, and an ultrafast-loading regime. In each of these regimes, the dependence of the bond strength on the loading rate is different. Thus, in order to expose the energy landscape that governs bond strength, molecular adhesion forces must be examined over an enormous span of time scales. A convincing experimental proof of these theoretical considerations was obtained in experimental measurements of biotin/avidin interaction forces (Merkel et al., 1999; Table 1).

It is worth noting that a different conclusion has been recently reached by Schwesinger et al. (2000) who studied the loading-rate-dependent unbinding forces for different series of ligand–receptor pairs. It was reported that for nine different fluorescein–anti-fluorescein antibody pairs

Table 1  
Interaction forces between ligand and receptor pairs

Molecular partners	Experimental setup	Specificity controls	Average forces (pN)	Reference
Avidin/biotin	Biotinylated bovine serum albumin (BSA) adsorbed on tip, with subsequent avidin adsorption; surface is biotinylated	Free avidin, free biotin, free BSA; biotin-coated tips	15,000–2000 <sup>a</sup>	Moy et al. (1994b)
Avidin/biotin Streptavidin/biotin	Biotinylated BSA adsorbed on tip, with subsequent avidin or streptavidin adsorption; ligand (biotin or derivatives) immobilized on surface	Immobilized biotin derivatives; low or high pH	~160 ~260	Moy et al. (1994a)
Avidin/biotin or derivatives	Biotinylated BSA adsorbed on tip, then incubated with avidin; biotinylated agarose beads as substrate	Free avidin or biotin in medium	~160	Florin et al. (1994)
Biotin/streptavidin	Biotinylated BSA adsorbed on glass microspheres (glued to cantilevers) and mica surface; surface further incubated with streptavidin	BBSA surface (no streptavidin); streptavidin surface blocked with biotin	~340	Lee et al. (1994b)
Biotin/streptavidin site-directed mutants	Biotinylated BSA adsorbed on tip and mica surface; surface further incubated with wild-type or mutant streptavidin	Free biotin in medium	Between 100 and 450 for mutants	Chilkoti et al. (1995)
Biotin/antibiotin antibody (Ab)	Biotinylated BSA covalently bound to tip via linker; Ab covalently bound to surface via linker; also reverse configuration	Non-biotinylated BSA on tip; biotin and streptavidin in medium; non-specific Ab on surface; low or high pH	~110	Dammer et al. (1996)
Biotin/streptavidin	Biotin covalently bound to nanotube tips; streptavidin linked to surface by biotin groups	Free biotin in medium; unmodified nanotube tips	~200	Wong et al. (1998)
Fluorescein/antifluorescein single-chain Ab	Fluorescein covalently bound via linker to tip; Ab attached to gold surface by engineered C-terminal cysteine	Free fluorescein	~50	Ros et al. (1998)
Biotin/streptavidin or avidin	Biotin covalently attached via linkers to glass micro-beads and surfaces; avidin was further adsorbed to both, such that free biotin groups were still available for infrequent bond formation	Linkers terminated in chemical groups inactive in attaching biotin; free biotin	Between 5 and 170, depending on loading rate	Merkel et al. (1999)

<sup>a</sup> Number of interacting molecular pairs estimated to be ~100.

Table 2

Interaction forces between various pairs of protein

Molecular partners	Experimental setup	Specificity controls	Average forces (pN)	Reference
<i>Antigen/antibody (Ag/Ab)</i>				
IgG-Ab/protein G	Biotinylated BSA adsorbed on tip, with subsequent avidin adsorption; further functionalization of above tip with biotinylated IgG-Ab; surface is protein G-covered	Free protein G	3000–4000 <sup>a</sup>	Moy et al. (1994b)
Fluorescein/antifluorescyl Ab	Fluorescein covalently bound to a silica bead glued to cantilever; Ab covalently bound to surface	Non-specific Ab on surface; non-derivatized tip; <sup>b</sup> no protein on surface	~200 <sup>c</sup>	Stuart and Hlady (1995)
Anti-human serum albumin/human serum albumin	Covalently bound Ab to tip and Ag to surface via long flexible spacers	Free serum albumin in medium	~250	Hinterdorfer et al. (1996)
Ferritin/antiferritin Ab	Both Ag and Ab covalently attached to tip and surface, respectively	Non-functionalized tip and tips at different stages of chemical treatment used for immobilization; non-specific Ab on surface	~50	Allen et al. (1997)
Anti-intercellular adhesion molecule-1 (ICAM-1)/ICAM-1	Covalently bound Ab to tip and Ag to surface via long flexible spacers		~100	Willemsen et al. (1998)
<i>Other protein/protein interactions</i>				
Actin/actin in actin filaments			Not given	Moy et al. (1994a)
Cell adhesion proteoglycans	Proteoglycans covalently attached to organic monolayers on tip and surface through the protein moiety	Surfaces covered with monolayers; Ca <sup>2+</sup> or Mg <sup>2+</sup> in various concentrations; monoclonal Ab to a carbohydrate epitope and a non-specific Ab	Up to 400; polyvalent binding with steps of 40	Dammer et al. (1995)
Insulin/insulin	Monomers covalently attached to both tips and surface via specific residues in ways to either favor or disfavor dimer formation	Free insulin; anti-insulin Ab	1300 <sup>d</sup>	Yip et al. (1998)
Two protein substrates citrate synthase or $\beta$ -lactamase/ <i>E. coli</i> chaperonin GroEL	Protein substrates covalently bound to tip; GroEL adsorbed to mica with the substrate binding site on top	Native or denatured substrates; presence or absence of ATP; bare mica or non-functionalized hydrophilic or hydrophobic tips	~240 and ~420 for lactamase, and citrate synthase, respectively	Vinckier et al. (1998)

Table 2 (continued)

Molecular partners	Experimental setup	Specificity controls	Average forces (pN)	Reference
Recombinant P-selectin/P-selectin glycoprotein ligand-1 (PSGL-1)	Biotinylated P-selectin attached to avidin-coated coverslips; biotinylated PSGL-1 attached to avidin-coated tips	Buffer supplemented with EDTA, instead of $\text{Ca}^{2+}$ ; non-glycosylated or glycosylated PSGL-1	~160	Fritz et al. (1998)
Myelin basic protein/lipid bilayers	Lipid adsorbed to surface and further incubated with myelin; tip coated with myelin	Bare mica surface or surface with adsorbed lipid; low or high ionic strength	~140 <sup>e</sup>	Mueller et al. (1999)

<sup>a</sup> Number of interacting molecular pairs not determined.

<sup>b</sup> Large discontinuities in the force curves were observed in the first two controls and attributed to non-specific discrete interactions between protein and the AFM spherical bead tip.

<sup>c</sup> Measured within 2 s of initial contact; extended contact leads to increased forces.

<sup>d</sup> Multiple unbinding events and elongation of monomer prior to dissociation.

<sup>e</sup> No elastic stretching in myelin when on lipid, in contrast to when on mica.

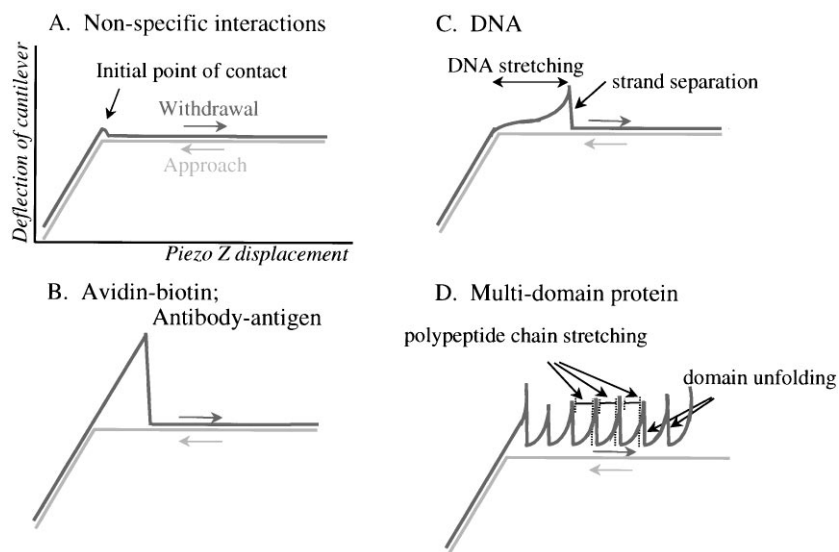


Fig. 5. Illustration of the major types of force curves obtained as a result of different types of interactions between biological macromolecules. (A) A control curve recording the non-specific interactions between an AFM tip and a hard surface. (B) Curve reflecting specific ‘adhesion’ interactions between pairs of molecular partners immobilized on the tip and surface, respectively. Such curves have been recorded in the case of biotin–avidin (or streptavidin) interactions, and in the case of antigen–antibody interactions (see Tables 1 and 2). (C) Force curve obtained upon stretching of DNA. Note the different shape of the curve in the portion preceding the jump-off-contact. This shape can be fitted by the worm-like chain model and results from the elastic stretching of the DNA from B- to S-conformation (see text). The jump-off-contact reflects the melting of the DNA duplex. (D) Typical force curves obtained on stretching of multi-domain proteins (for schematic interpretation of such multi-peak curves see Fig. 6). Similar multi-peak curves with somewhat less regular appearance are obtained upon stretching of chromatin (see text).

the measured unbinding forces correlated well with the respective thermal off-rates in solution; the dependence of the force on the logarithm of the loading rates was linear over six orders of magnitude of the latter parameter. The authors attribute the difference between their results and those from Evans' laboratory (see above) to certain atypical structural features of the avidin/biotin pair.

### 3.2. *Protein/protein interactions*

The second populated class of intermolecular force measurements involved protein/protein interactions, including the highly specific antigen/antibody interactions (Table 2). Again, the variety of experimental setups was wide, and the molecular pairs studied were very diverse with respect to their structure and their physiological functions. Once again, since different loading regimes have been used by different investigators, it is not straightforward to directly compare the measured interaction forces.

### 3.3. *Interactions between complementary strands of DNA*

The interactions between the two strands of a double-helical DNA molecule may also be classified as intermolecular interactions, and should, as such, be discussed in this section. In a pioneering work, Lee et al. (1994a) measured the interaction forces between complementary 20-base strands covalently immobilized to a silica probe and surface. The sequence of the oligonucleotides was designed so that they did not contain self-complementary regions, and base pairing was restricted to the formation of duplexes of discrete lengths: 20, 16, 12, 8 and 4 bp (only the first three of these were expected to be thermodynamically stable). Non-complementary oligonucleotides served as specificity controls. Measurements of interaction force gave  $\sim 70$  pN per base pair.

In a different experimental approach, Boland and Ratner (1995) used self-assembled purines and pyrimidines on planar gold surfaces and gold-coated AFM tips. Specific hydrogen-bonding interactions between the molecules on the tip and surface could only be measured when complementary base pairing could take place. A rupture force of 54 pN was reported for a single AT pair, close to the value reported by Lee et al. (1994a). These values are much higher than the value of 10–15 pN per base pair reported from the unzipping experiments of Essevaz-Roulet et al. (1997) performed using bendable micro-needles as force sensors. A possible explanation for this discrepancy could lie in the significant non-specific interactions between the tip and the surface in the AFM setup, as discussed by Samori (1998).

More recently, Noy et al. (1997a) have used self-assembled monolayers for immobilizing complementary 14-mers to gold-coated tip and surface. With increasing applied force, the final separation of the complementary strands proceeded after DNA stretched to a stable form of approximately twice the length of the B-form. This structural transition of double-stranded DNA from the B-form to the so-called S- (stretched) form was first identified in long DNA molecules in experiments using optical fibers (Cluzel et al., 1996) and optical tweezers (Smith et al., 1996). It is worth noting that the structural transition to the extended, S-form DNA in the AFM experiments was observed at a force of  $120 \pm 50$  pN, close to the value of 140 pN estimated from modeling studies (Lebrun and Lavery, 1996), and much higher than the force measured in both the optical tweezers and optical fibers experiments ( $\sim 70$  pN). The adhesion forces between the complementary oligonucleotides were distributed around  $460 \pm 180$  pN.

A similar sequence of structural transitions — stretching followed by melting — has been recently reported for a restriction fragment of  $\lambda$ -DNA stretched with the AFM (Rief et al., 1999a). The force for the stretching transition was found to be 65 pN, and that for the melting  $\sim$ 150 pN. Stretching poly(dG–dC) and poly(dA–dT) allowed the expected sequence dependence of melting to be directly demonstrated, with base pair unbinding force for G–C of  $\sim$ 20 pN, and that for A–T of  $\sim$ 9 pN. Evidently, more work is needed to resolve some apparent inconsistencies among the results obtained in different laboratories, and between experimental measurements and theory.

### 3.4. *Stretching chromatin*

Finally, the AFM has been used to stretch chromatin fibers, with the goal of determining the forces needed to break the bonds between the DNA and the histone octamers in the nucleosomal particles. Such studies are of particular importance since processes like transcription, replication, and repair that use DNA as a template must, in one way or another, move the histones out of the way of the corresponding enzymatic machineries. Stretching of native chromatin fibers isolated from chicken erythrocyte nuclei (Leuba et al., 1999) produced complex multi-peak patterns, reminiscent of those obtained on stretching multi-domain proteins (see below). Moreover, the presence or absence of linker histones in the fiber affected the magnitude of the peaks (Leuba et al., 1999). In order to understand the complex force curves obtained on native chromatin fibers, we switched to a defined system: chromatin fibers of relatively regular structure obtained by reconstituting a tandemly repeated nucleosome positioning DNA sequence with core histones (Leuba et al., 2000). Stretching such arrays of 12 nucleosomes produced force curves containing one or more peaks, with peak-to-peak distances much too small to arise from unraveling of the nucleosomal DNA from around the histone octamer. Careful analysis of the data led to the conclusion that, under the experimental conditions used, nucleosomes did not unravel even at forces exceeding 300 pN. The most likely explanation of these results is that the linker DNA (the DNA connecting nucleosomes) stretches under the applied tension, followed by detachment of the individual nucleosome from the surface. Further experiments are in progress to study chromatin behavior under applied tension.

It should be noted that chromatin fibers have been recently stretched using optical tweezers. Cui and Bustamante (2000) pulled on long stretches of chicken erythrocyte chromatin fibers, whereas Bennick et al. (submitted) directly reconstituted single chromatin fibers on  $\lambda$ -DNA molecules already attached between two polystyrene beads in the liquid cell of the apparatus. Both groups observed irreversible changes in fiber structure when the stretching force exceeded 20 pN. The data resolution in the Bennick et al. experiments was high enough to allow measurements of individual opening events that were attributed to the unraveling of individual nucleosomes in the chromatin fiber. It is highly desirable to compare the forces measured in the optical tweezers experiments and those obtained in the AFM; such a comparison may become possible after slight modifications of the experimental setup presently used in our AFM experiments.

## 4. **Intramolecular structural transitions in polysaccharides, DNA, and multi-domain proteins**

The AFM has proven particularly useful in studying intramolecular interactions. We have already mentioned the stretching of the DNA double helix that precedes its melting. A major

research effort has focused on the unfolding of multi-domain protein molecules or of individual protein domains. The interested reader may greatly benefit from the several recent enlightening reviews covering this area (Fisher et al., 1999a, b; Carrion-Vazquez et al., 2000). We will limit ourselves to schematically illustrating the principle of these experiments (Fig. 6), and to summarizing the available literature in a table format (Table 3).

At small extensions (relative to the chain length), polymers generate a restoring force that is mainly entropic in origin. If force is applied to a polymer chain, an opposing force is created as a result of the reduction in entropy. The behavior of polymers under mechanical stress has been described by the worm-like chain model of elasticity (Flory, 1989), with the persistence length and the contour length comprising the adjustable parameters of the model. A particularly well-studied example of an entropic elastic polymer is DNA stretched at forces up to 65 pN (Bustamante et al., 1994; Marko and Siggia, 1995). The behavior of DNA, however, deviates from entropic elasticity at relatively high forces: application of forces above a certain threshold level to DNA leads to conformational changes beyond simple straightening of the chain and results in extensions beyond the contour length. As mentioned before, DNA undergoes a stretching B- to S-transition above 65 pN (Cluzel et al., 1996; Smith et al., 1996; Noy et al., 1997a; Rief et al., 1999a).

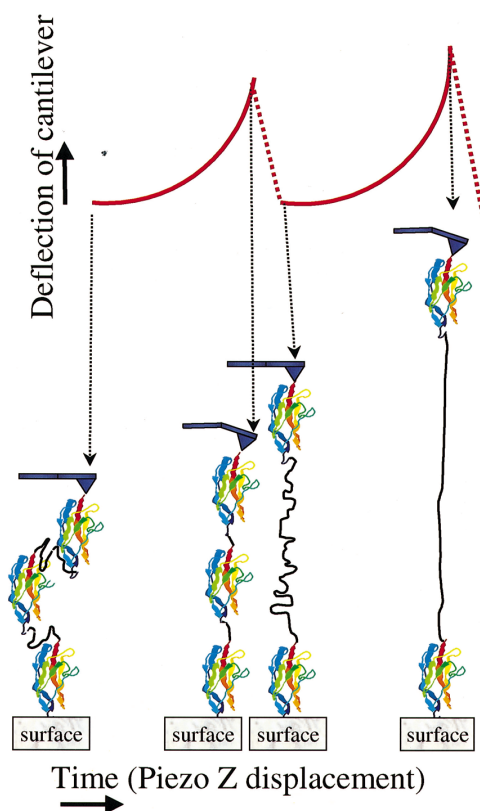


Fig. 6. Schematic showing the structural transitions in multi-domain proteins giving rise to the multi-peak force curves, as those represented in Fig. 5D.

Table 3  
Stretching of multi-domain proteins

Native protein, recombinant fragment, or polyhomodomain	Structure of the protein	Extension per sub-unit/domain ( $\Delta L_c$ )	Average force (pN)	Reference
$\alpha_2$ -macroglobulin	Four identical subunits, each of 1451 aa, containing 11 intra- and 2 inter-subunit SS bonds	150 nm for each of four identical subunits; such an extension is possible without breaking the SS bonds	> 250	Mitsui et al. (1996)
Titin (native protein or recombinant fragments containing 8 or 4 immunoglobulin (Ig-like domains)	Ig-like and fibronectin (Fn)-III-like tandemly repeated domains	25–28 nm	150–300	Rief et al. (1997a)
Titin (recombinant fragments from different parts of the molecule containing 6–8 Ig- or Fn-III-like domains)	Ig-like and Fn-III like tandemly repeated domains	28.2–31.5 nm	180–240 <sup>a</sup>	Rief et al. (1998)
Tenascin (native protein or recombinant fragment containing 15 Fn-III-like domains)	SS-linked hexamers, each made of tandemly repeated epidermal growth factor-like and Fn-III-like domains. Fn-III domain is a seven-stranded $\beta$ -barrel, similar to that of Ig-like domains	28.5 nm	~140	Oberhauser et al. (1998)
Twelve identical repeats of the Ig-like domain 27 of titin [(I27) <sub>12</sub> ]	$\beta$ -barrel consisting of seven $\beta$ -strands; H-bonds perpendicular to the direction of applied force			Carrion-Vazquez et al. (1999) and Marszalek et al. (1999)
Wild type		24.8 nm (75 amino acids)	~200–210	
Mutants containing clusters of five glycines inserted				
In the folded region		1.9 nm (5 amino acids) increase over wild type		
Outside the folded region		No increase		
Twelve identical repeats of the Ig-like			~265 <sup>b</sup>	Marszalek et al. (1999)

Table 3 (continued)

Native protein, recombinant fragment, or polyhomodomain	Structure of the protein	Extension per sub-unit/domain ( $\Delta L_c$ )	Average force (pN)	Reference
domain 28 of titin [(I28) <sub>12</sub> ]				
Nine identical repeats of the C2A domain of synaptotagmin I[(C2A) <sub>9</sub> ]	$\beta$ -barrel with N- and C-terminal ends pointing in the same direction; H-bonds parallel to the direction of applied force	38 nm (106 amino acids)	~60	Carrion-Vazquez et al. (2000)
Spectrin (native protein or recombinant fragment) containing repeats 13–18; $\alpha$ -actinin (four spectrin-like domains $\alpha 1$ – $\alpha 4$ )	Spectrin contains homologous repeats; each repeat forms a triple-helical, anti-parallel coiled-coil	31.7 nm	~25–35	Rief et al. (1999b)
Four identical repeats of a rat calmodulin domain CaM <sub>4</sub>	Seven $\alpha$ -helices in dumbbell shape; homogeneous distribution of intrahelix H-bonds	The protein extends in one step; 225 nm	~600	Carrion-Vazquez et al. (2000)

<sup>a</sup> Although structurally highly homologous, the Fn-III-like domains of titin and tenascin unfold at different forces: 180–200 pN for titin, and only ~110 pN for tenascin.

<sup>b</sup> Each complete unfolding of a domain is preceded by a fast initial extension of ~7 Å which reflects the existence of an unfolding intermediate.

A well-expressed deviation from entropic elasticity in the high-force stretching regime has also been observed for certain polysaccharides (Rief et al., 1997b; Marszalek et al., 1998). This deviation was attributed to either twisting and bending of bond angles (Rief et al., 1997b), or to chair–boat transitions of the glucopyranose ring of the stretched polysaccharide (Marszalek et al., 1998).

Stretching of multi-domain proteins presents an even more complicated case, where the force–extension curves are strings of successive enthalpic and entropic portions, reflecting the unfolding of individual domains in the multi-domain polypeptide chain, followed by stretching of the unfolded domain (Fig. 6). As such proteins are elongated as a result of the initial application of force, they undergo a typical entropic stretching at the beginning. At a certain force, however, one of the folded domains unfolds, adding significant length to the chain and relaxing the stress on the cantilever, which returns to its non-deflected state. The denatured portion of the polypeptide chain can now undergo entropic stretching, behaving like a typical polymer chain. Further extension creates forces high enough to unfold a second domain, which is then stretched entropically, etc. The unfolding and stretching of each individual domain creates an individual peak in the force curve, leading to the characteristic saw-tooth pattern, illustrated in Figs. 5 and 6. Table 3 enumerates the reported studies performed on different protein substrates. Considerable progress in interpreting the force curves has been achieved through the use of recombinant

proteins consisting of identical, tandemly repeated folded domains (Table 3; see Fisher et al., 1999a, b; Carrion-Vazquez et al., 2000 and references cited therein), and of steered molecular dynamic simulations (Lu et al., 1998; Marszalek et al., 1999). An alternative way to interpret peaks in multi-peak force curves has been to image the material before and after pulling. For example, in the case of pulling well-defined two-dimensional bacterial surface layers, it has been possible to identify by subsequent imaging which bacterial pore domains have been unzipped from the close spatial association with neighboring subunits (Müller et al., 1999). These authors interpret the multiple, well-spaced peaks in a force curve as discrete extensions of the portions of the polypeptide chains that connect individual subunits. Using the same technique, Oesterhelt et al. (2000) were able to image purple membranes before and after extraction of individual bacteriorhodopsin molecules from the membranes. The force–extension curves were recorded after the initial imaging and interpreted in terms of sequential extraction and unfolding of individual  $\alpha$ -helices. Some of the seven transmembrane  $\alpha$ -helices constituting bacteriorhodopsin unfolded pair-wise, whereas others unfolded one by one; moreover, details in the structure of specific portions of the force curve allowed resolution of complex extraction and unfolding paths for some individual helices.

The data obtained thus far (Table 3) already allow some interesting insights into the stability of different domains. Folded  $\beta$ -barrel domains, such as the immunoglobulin-like domains of the giant muscle protein titin and the fibronectin-III-like domains of the extracellular matrix protein tenascin, unfold under high force, between 200 and 260 pN. Such a force is needed to simultaneously break several hydrogen bonds in the  $\beta$ -barrel that are situated perpendicularly to the direction of applied force. Another  $\beta$ -barrel, present in the C2A domain of the membrane protein synaptotagmin I, unfolds at lower forces; in this domain the hydrogen bonds stabilizing the structure are parallel to the direction of applied force, and are broken sequentially, requiring much lower force,  $\sim 60$  pN (Carrion-Vazquez et al., 2000). The triple-helical, coiled-coils in the folded domains of spectrin, a component of the membrane-associated skeleton in erythrocytes, unravel at even lower forces, between 25 and 35 pN (Rief et al., 1999b). In contrast to the  $\beta$ -barrel structures, the tertiary structure of the spectrin domain is not stabilized by hydrogen bonds (hydrogen bonds stabilize the  $\alpha$ -helices themselves but not the bundle as a whole); the hydrophobic interactions maintaining the integrity of the bundle structure are much weaker than the hydrogen bonds, and are thus ruptured at much lower force. Finally, proteins like calmodulin, although containing repeated folded domains, do not produce peaks in the force curves but behave as random elastic polypeptide chains under force (Carrion-Vazquez et al., 2000). Their “all  $\alpha$ ” domains that are stabilized by intrahelical hydrogen bonds do not resist unfolding, and the protein yields to force in one step. More recently it has been demonstrated with an artificial homopolymer of repeating  $\alpha$ -helical T4 lysozymes molecules that it is possible to observe small individual peaks per protein monomer (Yang et al., 2000).

## **5. Measuring the viscoelastic properties of biological structures and macromolecules**

It is clear that whenever the effective stiffnesses of the cantilever and the biological sample on the surface are comparable, and the probe is pushed into the sample, the sample undergoes measurable indentation of the local surface at the point of contact of the tip. When the stress

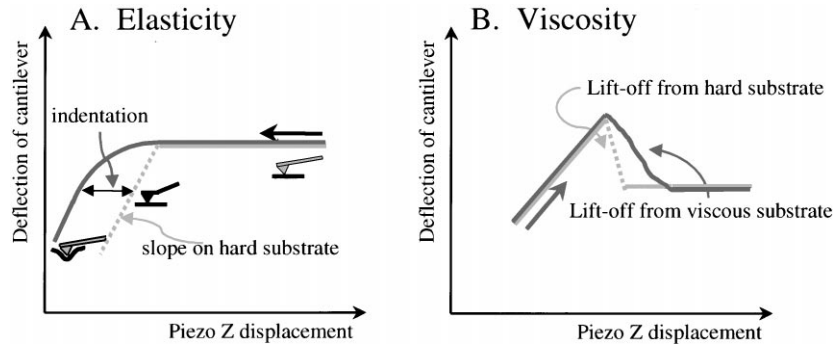


Fig. 7. Appearance of force curves when the sample indents under the tip (A) and when the jump-off-contact is slowed down due to viscosity of the sample (B).

(deformation force) and the strain (the amount of deformation) are linearly related, the deformation of the material is elastic, and the material will regain its original form upon relaxation. The depth of indentation can be used to measure local elasticity (Radmacher et al. (1992, 1994a, b) and Fritzsche and Henderson (1997); for reviews see Vinckier and Semenza (1998) and Heinz and Hoh (1999a)) in terms of Young's elastic modulus (the mechanical resistance of a material while elongating or compressing) (Fig. 7A). A detailed treatise of how AFM indentation data can be used to measure micromechanical properties of soft biological samples has been recently published (Costa and Yin, 1999).

The capability of AFM to provide information on the elastic properties of biological structures has been used to study different types of differentiated cells and organelles (for further references see Vinckier and Semenza, 1998; Heinz and Hoh, 1999a). The elastic modulus of thin films of gelatin was estimated to be  $0.02 \times 10^6$  Pa (Pascal or  $\text{N/m}^2$ ) (Domke and Radmacher, 1998), that of human chromosomes  $0.05\text{--}0.1 \times 10^6$  Pa (Ikai et al., 1997), of microtubules  $3 \times 10^6$  Pa (Vinckier et al., 1996), and that of lysozyme  $500 \times 10^6$  Pa (Radmacher et al., 1994b). The elastic modulus of DNA was shown to change with conformation of the molecule: B-DNA was characterized by a modulus of  $290 \times 10^6$  Pa, whereas the modulus of the stretched (S-form) was estimated to be  $2000 \times 10^6$  Pa, i.e., there was a 7-fold increase in the stiffness of the DNA double helix upon B- to S-transition (Noy et al., 1997a). For comparison, estimates from optical tweezers experiments gave a value of  $350 \times 10^6$  Pa for B-form DNA (Smith et al., 1996).

The behavior of soft biological samples shows another type of deviation from that of a hard surface, this time on the retraction curve. Whereas the lift-off occurs quickly on hard surfaces, it may be considerably slowed down in the case of soft biological samples (Fig. 7B). The lift-off speed may be used to estimate the viscosity of the sample (Radmacher et al., 1994b).

There is little doubt that the use of AFM for elasticity and viscosity measurements will be broadened in the future.

## 6. Measuring interactions between cells

Recently, force–distance curves have been also utilized to identify cell partners that interact specifically in certain biological reactions. By functionalizing AFM tips with whole cells of a given type and studying their interaction with monolayers of other cell types, it was possible to identify

the cell type in the uterine epithelium that interacts specifically with cells in the embryo during implantation (Thie et al., 1998). The technique introduced in this work offers novel approaches to the study of cell–cell interactions that are essential in many of the biological processes taking place in multicellular organisms.

## **7. Force maps**

Laterally resolved force curves can be recorded during raster scanning in the  $x$ – $y$  direction (Martin et al., 1987; Radmacher et al., 1994a, b; Baselt and Baldeschwieler, 1994). Individual curves can be assembled into a three-dimensional force volume (reviewed in Heinz and Hoh, 1999a). An alternative approach to producing spatially resolved force measurements is to create isoforce images across the sample, by assigning each point of the surface a separation distance at which a certain force is measured (Heinz and Hoh, 1999a). Collecting series of isoforce images at different forces can, in principle, reconstruct the same force volume as the one created by collecting individual laterally resolved force curves. The wealth of information in the force volume can be used to produce sample/surface maps reflecting different properties of the surface: adhesion, viscosity, elasticity, electrostatic interactions, etc. (e.g., Ludwig et al., 1997; Willemsen et al., 1998; Heinz and Hoh, 1999b).

A much faster approach to the point by point force curve measurement mentioned above has been to use the binding of a tethered antibody-modified tip to the substrate of the antibody to generate an effective force volume image (Raab et al., 1999). In this method, the image is distorted by enlarged widths and increased heights due to stretching of the antibody tether when the antibody binds the target antigen. This method permits location of the antigens, but quantitative force measurements require that a conventional force curve be acquired once the target is found in the image.

## **8. Concluding remarks**

It is becoming increasingly clear that AFM can be used in a variety of different applications to study biologically relevant inter- and intramolecular interactions. The field of force spectroscopy is in an exponential phase of development: each year we witness not only numerous new examples of applications, but also significant developments in instrumentation. There is little doubt that the AFM, combined with other techniques, such as the laser optical tweezers, will further promote our comprehension of the complexity and intricacy of molecular interactions in a way unperceivable until recently.

## **Acknowledgements**

We thank Dr. M. Karymov for discussion. S.H.L. is a National Cancer Institute Scholar.

## **References**

- Allen, S., Chen, X., Davies, J., Davies, M.C., Dawkes, A.C., Edwards, J.C., Roberts, C.J., Sefton, J., Tendler, S.J.B., Williams, P.M., 1997. Detection of antigen–antibody binding events with the atomic force microscope. *Biochemistry* 36, 7457–7463.

- Ashkin, A., 1997. Optical trapping and manipulation of neutral particles using lasers. *Proc. Natl. Acad. Sci. USA* 94, 4853–4860.
- Ashkin, A., Dziedzic, J.M., Yamane, T., 1987. Optical trapping and manipulation of single cells using infrared laser beams. *Nature* 330, 769–771.
- Baselt, D.R., Baldeschwieler, J.D., 1994. Imaging spectroscopy with the atomic force microscope. *J. Appl. Phys.* 76, 33–38.
- Bennick, U.L., Leuba, S.N., Leno, G.H., Zlatanova, J., de Grooth, B.G., Greve, J., Unfolding individual nucleosomes by stretching single chromatin fibres with optical tweezers. Submitted.
- Binnig, G., Quate, C.F., Rohrer, C., 1986. Atomic force microscope. *Phys. Rev. Lett.* 56, 930–933.
- Boland, T., Ratner, B.D., 1995. Direct measurement of hydrogen bonding in DNA nucleotide bases by atomic force microscopy. *Proc. Natl. Acad. Sci. USA* 92, 5297–5301.
- Burnham, N.A., Colton, R.J., Pollock, H.M., 1993. Interpretation of force curves in force microscopy. *Nanotechnology* 4, 64–80.
- Burnham, N.A., Kulik, A.J., 1998. Surface forces and adhesion. In: Bhushan, B. (Ed.), *Handbook of Micro/Nanotribology*. CRC Press, Boca Raton, FL.
- Bustamante, C., Marko, J.F., Siggia, E.D., Smith, S., 1994. Entropic elasticity of  $\lambda$ -phage DNA. *Science* 265, 1599–1600.
- Cappella, B., Baschieri, P., Frediani, C., Miccoli, P., Ascoli, C., 1997. Force–distance curves by AFM. *IEEE Engng. Med. Biol.* 16, 58–65.
- Cappella, B., Dietler, G., 1999. Force–distance curves by atomic force microscopy. *Surf. Sci. Rep.* 34, 1–104.
- Carrion-Vazquez, M., Marszalek, P.E., Oberhauser, A.F., Fernandez, J.M., 1999. Atomic force microscopy captures length phenotypes in single proteins. *Proc. Natl. Acad. Sci. USA* 96, 11288–11292.
- Carrion-Vazquez, M., Oberhauser, A.F., Fisher, T.E., Marszalek, P.E., Li, H., Fernandez, J.M., 2000. The mechanical topology of protein studied by AFM. *Prog. Biophys. Mol. Biol.*, 74, 63–91.
- Chen, G.Y., Warmack, R.J., Huang, A., Thundat, T., 1995. Harmonic response of near-contact scanning force microscopy. *J. Appl. Phys.* 78, 1465–1469.
- Chen, G.Y., Warmack, R.J., Thundat, T., Allison, D.P., Huang, A., 1994. Resonance response of scanning force microscopy cantilevers. *Rev. Sci. Instr.* 65, 2532–2537.
- Chilkoti, A., Boland, T., Ratner, B.D., Stayton, P.S., 1995. The relationship between ligand-binding thermodynamics and protein–ligand interaction forces measured by atomic force microscopy. *Biophys. J.* 69, 2125–2130.
- Cleveland, J.P., Manne, S., Bocek, D., Hansma, P.K., 1993. A nondestructive method for determining the spring constant of cantilevers for scanning force microscopy. *Rev. Sci. Instr.* 64, 403–405.
- Cluzel, P., Lebrun, A., Heller, C., Lavery, R., Viovy, J.-L., Chatenay, D., Caron, F., 1996. DNA: an extensible molecule. *Science* 271, 792–794.
- Costa, K.D., Yin, F.C.P., 1999. Analysis of indentation: implications for measuring mechanical properties with atomic force microscopy. *J. Biomech. Engng.* 121, 462–471.
- Cui, Y., Bustamante, C., 2000. Pulling a single chromatin fiber reveals the forces that maintain its higher-order structure. *Proc. Natl. Acad. Sci. USA* 97, 127–132.
- Dammer, U., Hegner, M., Anselmetti, D., Wagner, P., Dreier, M., Huber, W., Guntherodt, H.-J., 1996. Specific antigen/antibody interactions measured by force microscopy. *Biophys. J.* 70, 2437–2441.
- Dammer, U., Popescu, O., Wagner, P., Anselmetti, D., Guntherodt, H.-J., Misevic, G.N., 1995. Binding strength between cell adhesion proteoglycans measured by atomic force microscopy. *Science* 267, 1173–1175.
- Domke, J., Radmacher, M., 1998. Measuring the elastic properties of thin polymer films with the atomic force microscope. *Langmuir* 14, 3320–3325.
- Engel, A., Lyubchenko, Y., Müller, D., 1999. Atomic force microscopy: a powerful tool to observe biomolecules at work. *Trends Cell Biol.* 9, 77–80.
- Essevaz-Roulet, B., Bockelmann, U., Heslot, F., 1997. Mechanical separation of the complementary strands of DNA. *Proc. Natl. Acad. Sci. USA* 94, 11935–11940.
- Evans, E., Berk, D., Leung, A., 1991. Detachment of agglutinin-bounded red blood cells. I. Forces to rupture molecular-point attachments. *Biophys. J.* 59, 838–848.
- Evans, E., Ritchie, K., 1997. Dynamic strength of molecular adhesion bonds. *Biophys. J.* 72, 1541–1555.

- Evans, E., Ritchie, K., 1999. Strength of a weak bond connecting flexible polymer chains. *Biophys. J.* 76, 2439–2447.
- Fisher, T.E., Marszalek, P.E., Oberhauser, A.F., Carrion-Vazquez, M., Fernandez, J.M., 1999a. The micro-mechanics of single molecules studied with atomic force microscopy. *J. Physiol.* 520, 5–14.
- Fisher, T.E., Oberhauser, A.F., Carrion-Vazquez, M., Marszalek, P.E., Fernandez, J.M., 1999b. The study of protein mechanics with the atomic force microscope. *Trends Biochem. Sci.* 24, 379–384.
- Florin, E.L., Moy, V.T., Gaub, H.E., 1994. Adhesion forces between individual ligand–receptor pairs. *Science* 264, 415–417.
- Flory, P.J., 1989. *Statistical Mechanics of Chain Molecules*. Hanser, Munich.
- Frisbie, C.D., Rozsnyai, L.F., Noy, A., Wrighton, M.S., Lieber, C.M., 1994. Functional group imaging by chemical force microscopy. *Science* 265, 2071–2074.
- Fritz, J., Katopodis, A.G., Kolbinger, F., Anselmetti, D., 1998. Force-mediated kinetics of single P-selectin/ligand complexes observed by atomic force microscopy. *Proc. Natl. Acad. Sci. USA* 95, 12283–12288.
- Fritzsche, W., Henderson, E., 1997. Mapping elasticity of rehydrated metaphase chromosomes by scanning force microscopy. *Ultramicroscopy* 69, 191–200.
- Gibson, C.T., Watson, G.S., Myhra, S., 1996. Determination of the spring constants of probes for force microscopy/spectroscopy. *Nanotechnology* 7, 259–262.
- Grandbois, M., Beyer, M., Rief, M., Clausen-Schaumann, H., Gaub, H.E., 1999. How strong is a covalent bond? *Science* 283, 1727–1730.
- Grigg, D.A., Russell, P.E., Griffith, J.E., 1992. Tip–sample forces in scanning probe microscopy in air and vacuum. *J. Vac. Sci. Technol. A* 10, 680–683.
- Hansma, P.K., Cleveland, J.P., Radmacher, M., Walters, D.A., Hillner, P.E., Bezannilla, M., Fritz, M., Vie, D., Hansma, H.G., Prater, C.B., Massie, J., Fukunaga, L., Gurley, J., Elings, V., 1994. Tapping mode atomic force microscopy in liquids. *Appl. Phys. Lett.* 64, 1738–1740.
- Heinz, W.F., Hoh, J.H., 1999a. Spatially resolved force spectroscopy of biological surfaces using the atomic force microscope. *Trends Biotechnol.* 17, 143–150.
- Heinz, W.F., Hoh, J.H., 1999b. Relative surface charge density mapping with the atomic force microscope. *Biophys. J.* 76, 528–538.
- Hinterdorfer, P., Baumgartner, W., Gruber, H.J., Schilcher, K., Schindler, H., 1996. Detection and localization of individual antibody–antigen recognition events by atomic force microscopy. *Proc. Natl. Acad. Sci. USA* 93, 3477–3481.
- Hoh, J.H., Cleveland, J.P., Prater, C.B., Revel, J.-P., Hansma, P.K., 1992. Quantized adhesion detected with the atomic force microscope. *J. Am. Chem. Soc.* 114, 4917–4918.
- Hutter, J.L., Bechhoefer, J., 1993. Calibration of atomic-force microscope tips. *Rev. Sci. Instr.* 64, 1868–1873.
- Ikai, A., Mitsui, K., Tokuoka, H., Xu, X.M., 1997. Mechanical measurements of a single protein molecule and human chromosomes by the atomic force microscope. *Mater. Sci. Engng. C* 4, 233–240.
- Israelachvili, J.N., 1992. *Intermolecular and Surface Forces*. Academic Press, New York.
- Kellermayer, M.S., Smith, S.B., Granzier, H.L., Bustamante, C., 1997. Folding–unfolding transitions in single titin molecules characterized with laser tweezers. *Science* 276, 1112–1116.
- Lebrun, A., Lavery, R., 1996. Modeling extreme stretching of DNA. *Nucleic Acids Res.* 24, 2260–2267.
- Lee, G.U., Chrisey, L.A., Colton, R.J., 1994a. Direct measurement of the forces between complementary strands of DNA. *Science* 266, 771–773.
- Lee, G.U., Kidwell, D.A., Colton, R.J., 1994b. Sensing discrete streptavidin–biotin interactions with atomic force microscopy. *Langmuir* 10, 354–357.
- Leuba, S.H., Karymov, M.A., Liu, Y.Z., Lindsay, S.M., Zlatanova, J., 1999. Mechanically stretching single chromatin fibers. *Gene Ther. Mol. Biol.* 4, 297–301.
- Leuba, S.H., Zlatanova, J., Karymov, M.A., Bash, R., Liu, Y.-Z., Lohr, D., Harrington, R.E., Lindsay, S.U., 2000. The mechanical properties of single chromatin fibers under tension. *Single Mol.* 1, 185–193.
- Li, Y.Q., Tao, N.J., Pan, J., Garcia, A.A., Lindsay, S.M., 1993. Direct measurement of interaction forces between colloidal particles using the scanning force microscope. *Langmuir* 9, 637–641.
- Lindsay, S.M., 2000. The scanning probe microscope in biology. In: Bonnell, D. (Ed.), *Scanning Tunneling Microscopy and Related Techniques*. Wiley, New York, in press.

- Liu, Y.Z., Leuba, S.H., Lindsay, S.M., 1999. Relationship between stiffness and force in single molecule pulling experiments. *Langmuir* 15, 8547–8548.
- Lu, H., Israilewitz, B., Krammer, A., Vogel, V., Schulten, K., 1998. Unfolding of titin immunoglobulin domains by steered molecular dynamics simulation. *Biophys. J.* 75, 662–671.
- Ludwig, M., Dettmann, W., Gaub, H.E., 1997. Atomic force microscope imaging contrast based on molecular recognition. *Biophys. J.* 72, 445–448.
- Marko, J.F., Siggia, E.D., 1995. Stretching DNA. *Macromolecules* 28, 8759–8770.
- Marszalek, P.E., Lu, H., Li, H., Carrion-Vazquez, M., Oberhauser, A.F., Schulten, K., Fernandez, J.M., 1999. Mechanical unfolding intermediates in titin modules. *Nature* 402, 100–103.
- Marszalek, P.E., Oberhauser, A.F., Pang, Y.P., Fernandez, J.M., 1998. Polysaccharide elasticity governed by chair–boat transitions of the glucopyranose ring. *Nature* 396, 661–664.
- Martin, Y., Williams, C.C., Wickramasinghe, H.K., 1987. Atomic force microscope-force mapping and profiling on a sub 100 D scale. *J. Appl. Phys.* 61, 4723–4729.
- Merkel, R., Nassoy, P., Leung, A., Ritchie, K., Evans, E., 1999. Energy landscapes of receptor–ligand bonds explored with dynamic force spectroscopy. *Nature* 397, 60–63.
- Mitsui, K., Hara, M., Ikai, A., 1996. Mechanical unfolding of  $\alpha_2$ -macroglobulin molecules with atomic force microscope. *FEBS Lett.* 385, 29–33.
- Moy, V.T., Florin, E.-L., Gaub, H.E., 1994a. Intermolecular forces and energies between ligands and receptors. *Science* 266, 257–259.
- Moy, V.T., Florin, E.-L., Gaub, H.E., 1994b. Adhesive forces between ligand and receptor measured by AFM. *Colloid Surf. A* 93, 343–348.
- Mueller, H., Butt, H.-J., Bamberg, E., 1999. Force measurements on myelin basic protein adsorbed to mica and lipid bilayer surfaces done with the atomic force microscope. *Biophys. J.* 76, 1072–1079.
- Müller, D.J., Baumeister, W., Engel, A., 1999. Controlled unzipping of a bacterial surface layer with atomic force microscopy. *Proc. Natl. Acad. Sci. USA* 96, 13170–13174.
- Müller, D.J., Engel, A., 1997. The height of biomolecules measured with the atomic force microscope depends on electrostatic interactions. *Biophys. J.* 73, 1633–1644.
- Müller, D.J., Engel, A., Amrein, M., 1997. Preparation techniques for the observation of native biological systems with the atomic force microscope. *Biosens. Bioelect.* 12, 867–877.
- Noy, A., Vezenov, D.V., Kayyem, J.F., Meade, T.J., Lieber, C.M., 1997a. Stretching and breaking duplex DNA by chemical force microscopy. *Chem. Biol.* 4, 519–527.
- Noy, A., Vezenov, D.V., Lieber, C.M., 1997b. Chemical force microscopy. *Annu. Rev. Mater. Sci.* 27, 381–421.
- Oberhauser, A.F., Marszalek, P.E., Erickson, H.P., Fernandez, J.M., 1998. The molecular elasticity of the extracellular matrix protein tenascin. *Nature* 393, 181–185.
- Oesterhelt, F., Oesterhelt, D., Pfeiffer, M., Engel, A., Gaub, H.E., Müller, D.J., 2000. Unfolding pathways of individual bacteriorhodopsins. *Science* 288, 143–146.
- Pierres, A., Benoliel, A.-M., Bongrand, P., 1996. Measuring bonds between surface-associated molecules. *J. Immunol. Methods* 196, 105–120.
- Putman, C.A., van der Werf, K.O., de Groot, B.G., van Hulst, N.F., Greve, J., 1994. Tapping mode atomic force microscopy in liquids. *Appl. Phys. Lett.* 64, 2454–2456.
- Raab, A., Han, W., Badt, D., Smith-Gill, S.J., Lindsay, S.M., Schindler, H., Hinterdorfer, P., 1999. Antibody recognition imaging by force microscopy. *Nat. Biotechnol.* 17, 901–905.
- Radmacher, M., Cleveland, J.P., Fritz, M., Hansma, H.G., Hansma, P.K., 1994a. Mapping interaction forces with the atomic force microscope. *Biophys. J.* 66, 2159–2165.
- Radmacher, M., Fritz, M., Cleveland, J.P., Walters, D.A., Hansma, P.K., 1994b. Imaging adhesion forces and elasticity of lysozyme adsorbed on mica with the atomic force microscope. *Langmuir* 10, 3809–3814.
- Radmacher, M., Tillmann, R.W., Fritz, M., Gaub, H.E., 1992. From molecules to cells: imaging soft samples with the Atomic Force Microscope. *Science* 257, 1900–1905.
- Rief, M., Clausen-Schaumann, H., Gaub, H.E., 1999a. Sequence-dependent mechanics of single DNA molecules. *Nat. Struct. Biol.* 6, 346–349.

- Rief, M., Gautel, M., Oesterhelt, F., Fernandez, J.M., Gaub, H.E., 1997a. Reversible unfolding of individual titin immunoglobulin domains by AFM. *Science* 276, 1109–1112.
- Rief, M., Gautel, M., Schemmel, A., Gaub, H.E., 1998. The mechanical stability of immunoglobulin and fibronectin III domains in the muscle protein titin measured by atomic force microscopy. *Biophys. J.* 75, 3008–3014.
- Rief, M., Oesterhelt, F., Heymann, B., Gaub, H.E., 1997b. Single molecule force spectroscopy on polysaccharides by atomic force microscopy. *Science* 276, 1295–1297.
- Rief, M., Pascual, J., Saraste, M., Gaub, H.E., 1999b. Single molecule force spectroscopy of spectrin repeats: low unfolding forces in helix bundles. *J. Mol. Biol.* 286, 553–561.
- Ros, R., Schwesinger, F., Anselmetti, D., Kubon, M., Schafer, R., Pluckthun, A., Tiefenauer, L., 1998. Antigen binding forces of individually addressed single-chain Fv antibody molecules. *Proc. Natl. Acad. Sci. USA* 95, 7402–7405.
- Sader, J.E., 1995. Parallel beam approximation for v-shaped atomic force microscope cantilevers. *Rev. Sci. Instr.* 66, 4583–4587.
- Sader, J.E., Larson, I., Mulvaney, P., White, L.R., 1995. Method for the calibration of atomic force microscope cantilevers. *Rev. Sci. Instr.* 66, 3789–3798.
- Sader, J.E., White, L., 1993. Theoretical analysis of the static deflection of plates for atomic force microscope applications. *J. Appl. Phys.* 74, 1–9.
- Samori, B., 1998. Stretching, tearing, and dissecting single molecules of DNA. *Angew. Chem. Int. Ed.* 37, 2198–2200.
- Sarid, D., 1991. *Scanning Force Microscopy*. Oxford University Press, New York.
- Schwesinger, F., Ros, R., Strunz, T., Anselmetti, D., Güntherodt, H.-J., Honegger, A., Jermutus, L., Tiefenauer, L., Plückthun, A., 2000. Unbinding forces of single antibody–antigen complexes correlate with their thermal dissociation rates. *Proc. Natl. Acad. Sci. USA*, 197, 9972–9977.
- Senden, T.J., Ducker, W.A., 1994. Experimental determination of spring constants in atomic force microscopy. *Langmuir* 10, 1003–1004.
- Siedlecki, C.A., Marchant, R.E., 1998. Atomic force microscopy for characterization of the biomaterial interface. *Biomaterials* 19, 441–454.
- Smith, S.B., Cui, Y., Bustamante, C., 1996. Overstretching B-DNA: the elastic response of individual double-stranded and single-stranded DNA molecules. *Science* 271, 795–799.
- Smith, S.B., Finzi, L., Bustamante, C., 1992. Direct mechanical measurements of the elasticity of single DNA molecules by using magnetic beads. *Science* 258, 1122–1126.
- Stuart, J.K., Hlady, V., 1995. Effects of discrete protein–surface interactions in scanning force microscopy adhesion force measurements. *Langmuir* 11, 1368–1374.
- Stuart, J.K., Hlady, V., 1999. Reflection interference contrast microscopy combined with scanning force microscopy verifies the nature of protein–ligand interaction force measurements. *Biophys. J.* 76, 500–508.
- Tendler, S.J.B., Davies, M.C., Roberts, C.J., 1996. Molecules under the microscope. *J. Pharm. Pharmacol.* 48, 2–8.
- Thie, M., Röspe, R., Dettmann, W., Benoit, M., Ludwig, M., Gaub, H.E., Denker, H.-W., 1998. Interactions between trophoblast and uterine epithelium: monitoring of adhesive forces. *Hum. Reprod.* 13, 3211–3219.
- Torii, A., Sasaki, M., Hane, K., Okuma, S., 1996. A method for determining the spring constant of cantilevers for atomic force microscopy. *Meas. Sci. Technol.* 7, 179–184.
- Vinckier, A., Dumortier, C., Engelborghs, Y., Hellems, L., 1996. Dynamic and mechanistic study immobilized microtubules with atomic force microscopy. *J. Vac. Sci. Technol. B.* 14, 1427–1431.
- Vinckier, A., Gervasoni, P., Zaugg, F., Ziegler, U., Lindner, P., Groscurth, P., Plückthun, A., Semenza, G., 1998. Atomic force microscopy detects changes in the interaction forces between GroEL and substrate proteins. *Biophys. J.* 74, 3256–3263.
- Vinckier, A., Semenza, G., 1998. Measuring elasticity of biological materials by atomic force microscopy. *FEBS Lett.* 430, 12–16.
- Wagner, P., 1998. Immobilization strategies for biological scanning probe microscopy. *FEBS Lett.* 430, 112–115.
- Willemsen, O.H., Snel, M.M.E., van der Werf, K.O., de Grooth, B.G., Greve, J., Hinterdorfer, P., Gruber, H.J., Schindler, H., van Kooyk, Y., Figdor, C.G., 1998. Simultaneous height and adhesion imaging of antibody–antigen interactions by atomic force microscopy. *Biophys. J.* 75, 2220–2228.
- Wong, S.S., Joselevich, E., Woolley, A.T., Cheung, C.L., Lieber, C.M., 1998. Covalently functionalized nanotubes as nanometre-sized probes in chemistry and biology. *Nature* 394, 52–55.

- Yang, G., Cecconi, C., Baase, W.A., Vetter, I.R., Breyer, W.A., Haack, J.A., Matthews, B.W., Dahlquist, F.W., Bustamante, C., 2000. Solid-state synthesis and mechanical unfolding of polymers of T4 lysozyme. *Proc. Natl. Acad. Sci. USA* 97, 139–144.
- Yip, C.M., Yip, C.C., Ward, M.D., 1998. Direct force measurements of insulin monomer–monomer interactions. *Biochemistry* 37, 5439–5449.
- Zhong, Q., Inniss, D., Kjoller, K., Elings, V.B., 1993. Fractured polymer/silica fiber surface studied by tapping mode atomic force microscopy. *Surf. Sci. Lett.* 290, L688–L692.